



Corrosion of Cu by a sulfate reducing bacterium in anaerobic vials with different headspace volumes

Wenwen Dou^{a,b,c}, Yanan Pu^a, Xiaomei Han^a, Yi Song^a, Shougang Chen^{a,*}, Tingyue Gu^{b,*}

^a Department of Materials Science and Engineering, Ocean University of China, Qingdao 266100, China

^b Department of Chemical and Biomolecular Engineering, Institute for Corrosion and Multiphase Technology, Ohio University, Athens, OH 45701, USA

^c Shandong Key Laboratory of Corrosion Science, Institute of Oceanology, Chinese Academy of Sciences, Qingdao 266071, China

ARTICLE INFO

Article history:

Received 11 October 2019

Received in revised form 20 January 2020

Accepted 29 January 2020

Available online 30 January 2020

Keywords:

Copper corrosion

SRB

H₂S

Headspace

Microbiologically influenced corrosion

ABSTRACT

Microbiologically influenced corrosion (MIC) of copper by *Desulfovibrio vulgaris*, a sulfate reducing bacterium (SRB), was investigated in anaerobic vials with a fixed broth volume of 40 mL but varied headspace volumes (10 mL, 85 mL, 160 mL). It was found that the headspace volume variation had a very large effect on the dissolved [H₂S] in the broth and the cell counts of planktonic and sessile cells, as well as Cu corrosion severity. A 16× smaller headspace led to a 1.6-fold increase in the dissolved [H₂S], a 13-fold decrease in sessile SRB cell count, a 32-fold decrease in planktonic cell count and a 3.7-fold increase of Cu weight loss. SEM images revealed that different headspace volumes caused different corrosion patterns on the immersed coupons. With a lower headspace volume, pitting corrosion was observed, while with a higher headspace volume, intergranular corrosion was seen. The results confirmed that SRB MIC of Cu belongs to metabolite-MIC (M-MIC) by H₂S, unlike SRB MIC of carbon steel that belongs to extracellular electron transfer-MIC (EET-MIC) that is directly correlated with sessile cell counts rather than dissolved [H₂S].

© 2020 Elsevier B.V. All rights reserved.

1. Introduction

Corrosion is a naturally occurring phenomenon that costs huge economic losses to many industries [1]. Around US\$4 trillion was lost due to corrosion globally each year [2]. Microbiologically influenced corrosion (MIC) was recognized as early as 1910 [3]. It is reported that MIC is behind 20% of all corrosion losses and is involved in 50% of all pipeline failures [4–6]. MIC is an electrochemical process involving interactions of the material (often a metal), metabolites and microorganisms [7–9]. Multidisciplinary knowledge such as electrochemistry, microbiology, chemical engineering and corrosion engineering are needed to investigate MIC mechanisms, making it difficult topic [10]. MIC has already become a major threat in many industries such as oil and gas, water utilities and medical implant industry [11–14]. A good understanding of MIC mechanisms is essential for MIC case analyses and mitigation strategies. It has challenged corrosion and bioscience researchers for decades [15–21].

The microorganisms causing MIC include sulfate reducing bacteria (SRB), sulfur/sulfide oxidizing bacteria, nitrate reducing

bacteria, acid producing bacteria, iron oxidizing bacteria, and so on [22–25]. Among these microorganisms, SRB are often found responsible for MIC damages because of the prevalence of sulfate in anaerobic environments [26,27]. The greatest numbers of recorded corrosion problems have been associated with SRB in oil-field cases, far more than any other microorganisms [28].

In the past decades, considerable advances have been made in MIC mechanisms. Various mechanisms were proposed to explain different MIC processes [29–32]. MIC caused by microbes under anaerobic condition has been lumped into two distinct types: extracellular electron transfer MIC (EET-MIC) and metabolite MIC (M-MIC) [33–36]. EET-MIC relies on direct electron transfer (DET) or mediated electron transfer (MET) to transport extracellular electrons from outside cells, such as sulfate reducing bacteria and nitrate reducing bacteria cells, to inside the cells for respiration of sulfate and nitrate, respectively. With DET, bacteria cells obtain electrons either from a metal surface to electroactive *c*-cytochrome proteins on bacterial outer cell walls that are in direct contact with the metal surface or a semi-conductive corrosion product film such as an iron sulfide film on the metal, or with the help of conductive nanowires (type IV proteinaceous pili) [33,36]. DET has been widely investigated in microbial fuel cell (MFC) research. For

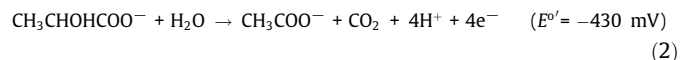
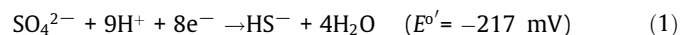
* Corresponding authors.

E-mail addresses: sgchen@ouc.edu.cn (S. Chen), gu@ohio.edu (T. Gu).

example, the pili of *Geobacter sulfurreducens* have been proven highly conductive which are used for EET by the bacterium [37].

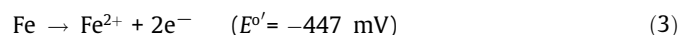
Some bacteria are normally incapable of EET. However, they are able to utilize soluble electron mediators for EET [38]. These redox active electron mediators serve as electron shuttles between a metal surface and bacteria in a biofilm that is a short distance away. Electron mediators have been used to enhance EET for improved MFC performances [39]. Zhang et al. and Jia et al. demonstrated that flavin adenine dinucleotide (FAD) and riboflavin, which are two very common electron mediators used by many microbial species, accelerated stainless steel and carbon steel MIC by sulfate reducing *Desulfovibrio vulgaris* and nitrate reducing *Pseudomonas aeruginosa*, respectively [40,41]. The classical cathode depolarization theory is the first electrochemical mechanism that explains the MIC of carbon steel by hydrogenase-positive SRB [29]. It has been modified by Gu et al. to show that it explains EET-MIC using $2\text{H}^+/\text{H}_2$ as an electron shuttle system for electron transfer [36]. Recently, Huang et al. proved that phenazine-1-carboxamide produced by *P. aeruginosa* is an electron mediator that plays an important role in the MIC by *P. aeruginosa*. When the gene for this molecule is knocked out, *P. aeruginosa* has a much reduced ability to corrode, while the gene's restoration in the knockout strain allows *P. aeruginosa* to regain its corrosion ability [42].

SRB utilize sulfate as the terminal electron acceptor for respiration to get energy from an electron donor such as lactate. Sulfate reduction in Reaction (1) coupled with lactate oxidation in Reaction (2) is thermodynamically favorable, meaning energy is released [43].



$E^{\circ'}$ represents the reduction potential at 25 °C, pH 7 and 1 M solutes (1 bar gasses) except H^+ vs. standard hydrogen electrode (SHE).

Xu et al. proved that SRB can use elemental iron as a replacement electron donor for energy production. They showed that pre-grown SRB biofilms on carbon steel become more aggressive under subsequent lactate starvation [44]. The reduction potentials of Fe^{2+}/Fe and acetate + $\text{CO}_2/\text{lactate}$ are similar, which means that Fe is as energetic as lactate.



HS^- is a characteristic metabolite of SRB respiration. It can combine with H^+ to form H_2S as shown in Reaction (4). In an anaerobic vial, some H_2S in the broth will escape to the headspace to establish an equilibrium with dissolved $[\text{H}_2\text{S}]$ in the liquid phase.

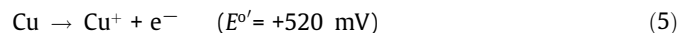


Sulfide is known to be toxic to most life forms including SRB. When a SRB culture has a larger headspace to broth volume ratio, more H_2S escapes to the gas phase, thus decreasing the dissolved $[\text{H}_2\text{S}]$ and reducing the sulfide toxicity in the broth. Jia et al. [45] found that increasing the ratio from 0.25 to 4 led to an increased number of sessile cells on carbon steel and thus accelerated carbon steel weight loss by as much as 200%. In a more recent work, Jia et al. [46] revealed that increasing $[\text{Fe}^{2+}]$ in the ATCC 1249 culture medium from 25 ppm (w/w) to 200 ppm in anaerobic vials without a headspace volume variation detoxified H_2S by countering the iron sulfide precipitation loss of Fe^{2+} that is a co-factor needed for two key enzymes in SRB metabolism. As a result, SRB grew better with concomitant increases in $[\text{H}_2\text{S}]$ and iron sulfide precipitation. As a consequence of a sessile cell count increase of 4.7 times,

the carbon steel weight loss increased by 5 times. In the two cases above, despite the opposite trends in $[\text{H}_2\text{S}]$ and iron sulfide precipitation, the increased corrosion is understandable because SRB MIC of carbon steel is EET-MIC [47]. With more sessile cells harvesting electrons from elemental iron in carbon steel, weight loss increases. With near-neutral broth pH in these two cases, H_2S corrosion was not a direct causal factor for weight loss [36,46].

Copper is widely used in heat exchangers, water cycling systems and nuclear waste storage systems [48–53]. Cu is highly resistant to oxygen corrosion but not to MIC. Many Cu MIC problems and investigations have been reported in the literature [54–57]. Dry walls in households contaminated with SRB caused corrosion of Cu water pipes and air-conditioning coils in Florida, USA [58]. Chen et al. found that SRB metabolism decreased the anodic zone area and localized corrosion was promoted in the presence of SRB [59]. Huang et al. reported that 70Cu-30Ni alloy corrosion was accelerated and intergranular corrosion occurred in anaerobic seawater contaminating SRB, and open circuit potential (OCP) shifted in the negative direction [60].

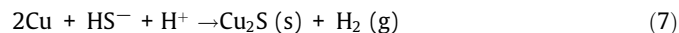
Unlike the Fe^{2+}/Fe couple with a rather negative reduction potential, Cu^+/Cu and Cu^{2+}/Cu have positive reduction potentials shown in reactions (5) and (6) that are much higher than that for sulfate reduction [61].



This means that Cu oxidation coupled with sulfate reduction is not thermodynamically favorable. Thus, Cu is not an energetic metal for SRB to harvest electrons to produce energy via dissimilatory sulfate reduction.

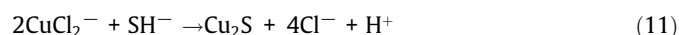
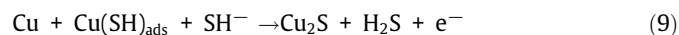
Recently, Dou et al. reported that SRB MIC weight loss of Cu is much higher than that of carbon steel [61]. The SRB MIC of Cu is mainly uniform corrosion accompanied by pitting corrosion with an *RPS* (relative pitting severity) close to unity, very different from the pitting corrosion in SRB MIC of carbon steel with an *RPS* much greater than unity.

Unlike Fe, Cu is not energetic. Thus, SRB cannot use electrons from elemental Cu for sulfate reduction to produce energy. This means SRB MIC of Cu cannot be EET-MIC. Instead, Cu can be corroded by sulfide and proton in the following reaction [57], which means SRB MIC of Cu belongs to M-MIC.



$$(\Delta G^{\circ'} = -58.3 \text{ kJ/mol})$$

Chen et al. proved that an intermediate product, $\text{Cu}(\text{SH})_{\text{ads}}$, formed on the copper surface before the generation of Cu_2S in the following reactions [50,62]:



$\text{Cu}(\text{SH})_{\text{ads}}$ accounts for the rapid drop of corrosion potential of the Cu electrode, while SH^- and Cl^- affect the structure of the corrosion products.

This work was specifically designed to study the impact of dissolved $[\text{H}_2\text{S}]$ and sessile cell count on SRB MIC of Cu by adjusting the headspace to broth volume ratio in anaerobic vials. The corrosion behaviors in the system with different headspace to broth volume ratios were compared with those of SRB MIC of

Fe to elucidate the fundamental differences between M-MIC and EET-MIC.

2. Experimental

2.1. Experimental materials, bacterium and chemicals

Pure 110 Cu (Cu > 99.9% by mass) (McMaster-Carr, Cleveland, OH, USA) was cut into 10 mm × 10 mm × 5 mm coupons. All the surfaces were painted with inert polytetrafluoroethylene except the top 10 mm × 10 mm working surface. The working surface was abraded to a final finish of 600-grit. *D. vulgaris* (ATCC 7757) was grown in ATCC 1249 culture medium with 196 ppm Fe²⁺ [47]. All chemicals were reagent grade from Sigma-Aldrich (St. Louis, MO, USA) or Fisher Scientific (Pittsburgh, PA, USA).

2.2. SRB incubation

Before incubation, the anaerobic vials and culture medium solutions (initial pH adjusted to 7.0) were sterilized at 121 °C for 20 min. The culture medium was deoxygenated with filter-sterilized argon gas via sparging for 1 h. A dissolved oxygen test kit (Product K-7540, CHEMetrics, Midland, VA, USA) was used to verify that the culture medium's dissolved oxygen level was below 40 ppb (w/w). One hundred ppm (w/w) filter-sterilized L-cysteine was used in the culture medium as an oxygen scavenger to remove residual dissolved oxygen and to counter possible minor oxygen ingress. All anaerobic manipulations were carried out in an anaerobic chamber.

Five replicate Cu coupons, 40 mL culture medium and 0.4 mL SRB seed culture were added to each vial before incubation at 37 °C for 7 days. The 50 mL, 125 mL and 200 mL (total volume) vials had 10 mL, 85 mL, 160 mL headspace volumes, respectively (Fig. 1), corresponding to headspace to broth volume ratios of 0.25:2.12:4.13. After the 7-day incubation, the Cu coupons were taken out to examine cell counts, corrosion products, coupon surface morphologies and weight losses.

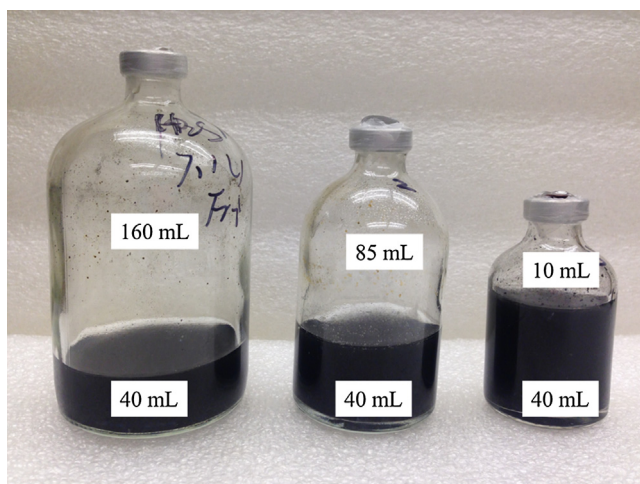


Fig. 1. Anaerobic vials containing Cu coupons, 40 mL culture medium and different headspace volumes (10 mL, 85 mL, 160 mL) after 7-day incubation in the weight loss experiment.

2.3. Characterizations of cells and corrosion

An SRB test kit with modified Postgate's B medium for SRB (Biotechnology Solutions, Houston, TX, USA) for most probable number (MPN) method was used to enumerate planktonic and sessile cells. For sessile cell counting, sessile cells were removed and suspended in a phosphate buffered saline (PBS) solution (KH₂PO₄ 0.27 g, Na₂HPO₄ 1.42 g, NaCl 8 g, KCl 0.2 g, deionized water 1 L, pH 7.4). Then, the cell suspension was enumerated just like a planktonic cell sample. Live and dead sessile cells on coupon surfaces were visualized under confocal laser scanning microscope (CLSM) (LSM 510, Carl Zeiss, Jena, Germany). Before observations, coupons were stained using the Live/Dead[®] BacLight™ Bacterial Viability Kit (Life Technologies, Grand Island, NY, USA) for 15 min.

On replicate coupons, biofilm morphology was examined under a scanning electron microscope (SEM) (JSM-6390, JEOL, Tokyo, Japan). The procedure for SEM sample preparation was reported elsewhere [63]. A 3D surface profilometer (ALC13, Alicona Imaging GmbH, Graz, Austria) was used to examine coupon surface profiles and to locate deepest pits. A 10% (v/v) H₂SO₄ solution was used to remove biofilms and corrosion products before weight loss and pit depth measurements according to ASTM G1-02 [64]. On the same coupons, the chemical compounds of the corrosion products were determined using an X-ray diffractometer (XRD) (Bruker D8 Discovery model, Bruker AXS GmbH, Karlsruhe, Germany). The H₂S concentration in the headspace of each anaerobic vial was obtained with a micro-gas chromatograph (micro-GC) instrument (Agilent 490, Agilent Technologies, Palo Alto, CA, USA) as described in a previous work [45].

2.4. Electrochemical tests

Electrochemical tests were performed in 450-mL glass cells with 290 mL culture medium to submerge electrodes. Headspace volumes of 10, 85 and 160 mL were achieved by putting inert glass beads in the glass cells to occupy unwanted space. In each glass cell, a Cu coupon with 10 mm × 10 mm surface exposed was used as the working electrode. A saturated calomel electrode (SCE) fitted with a Vycor tip placed close to the working electrode surface was used as the reference electrode. The counter electrode was a platinum mesh plate (20 mm × 20 mm). A potentiostat (VersaSTAT 3, Princeton Applied Research, Oak Ridge, TN, USA) with VersaStudio Version 3 software was used to perform electrochemical measurements. Linear polarization resistance (LPR) was tested by scanning from -10 mV to +10 mV with respect to the stabilized open circuit potential (OCP) at a rate of 0.167 mV/s. Electrochemical impedance spectroscopy (EIS) was measured in the frequency range from 10⁴ to 10⁻² Hz at stable OCP with a 10 mV amplitude sinusoidal alternate current voltage signal. Version 3.30d ZSimDemo software (EChem Software, Ann Arbor, MI, USA) was used to analyze the EIS spectra.

3. Results

3.1. Cell count, surface analysis and corrosion product analysis

Fig. 2 shows SRB sessile cell counts on Cu coupons and planktonic cell counts in the anaerobic vials with different headspace volumes after the 7-day incubation. The sessile cell count and the planktonic cell count both increased when the headspace volume increased from 10 mL to 160 mL. Fig. 3 shows the CLSM images of the sessile SRB cells on Cu coupons. With the increase

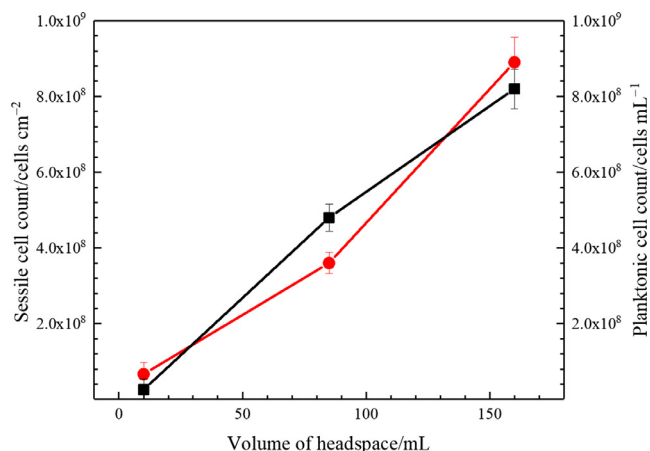


Fig. 2. SRB sessile cell counts (circle) on Cu coupons and planktonic cell counts (square) in culture media after 7-day incubation in anaerobic vials with different headspace volumes (10 mL, 85 mL, 160 mL).

of the headspace volume, there were more sessile cells, supporting the trend shown in Fig. 2.

Fig. 4(a-c) shows the Cu surface morphology before removing biofilms and corrosion products. For 10 mL headspace (Fig. 4a), the surface morphology contained large crystalline grains about 30–40 μm in size. Small chips and lamellar crystal particles were present for 85 mL headspace and for 160 mL headspace as shown in Fig. 4(b,c). They were clustered into petal shapes with a diameter of 10 μm . After surface cleaning, uniform corrosion accompanied with corrosion pits are clearly seen in Fig. 4(a',a'') for 10 mL headspace. For 85 mL headspace and 160 mL headspace, grain boundary corrosion is clearly seen in Fig. 4(b',c''). The corroded grain boundaries were dotted with small corrosion pits.

Fig. 5 shows the surface profiles of Cu obtained from the profilometer after removing corrosion products. The largest pit depth was found to be 23.5 μm for 10 mL headspace. The surface profiles for 85 mL headspace and for 160 mL headspace did not have clear-cut large pits, which is corroborated by the SEM images (Fig. 4).

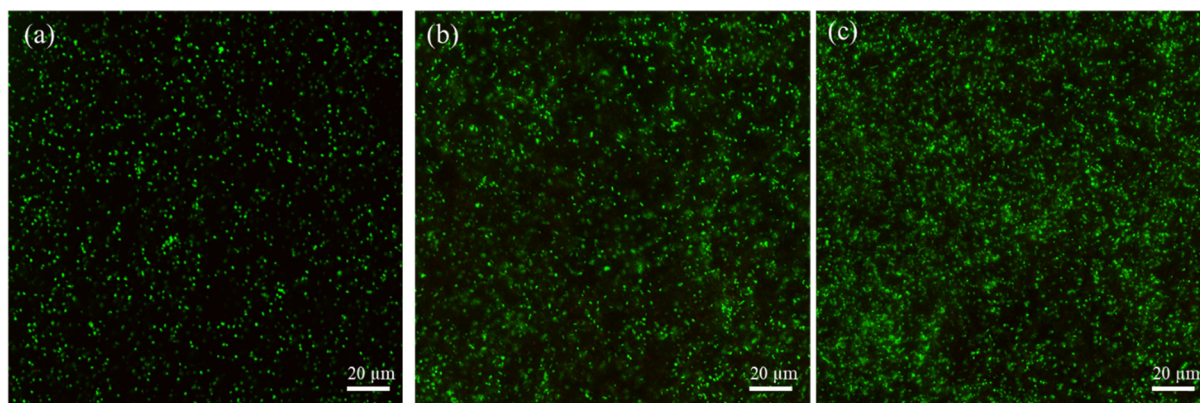


Fig. 3. CLSM images of SRB sessile cells on Cu coupons after 7-day incubation in anaerobic vials with different headspace volumes: (a) 10 mL, (b) 85 mL, (c) 160 mL.

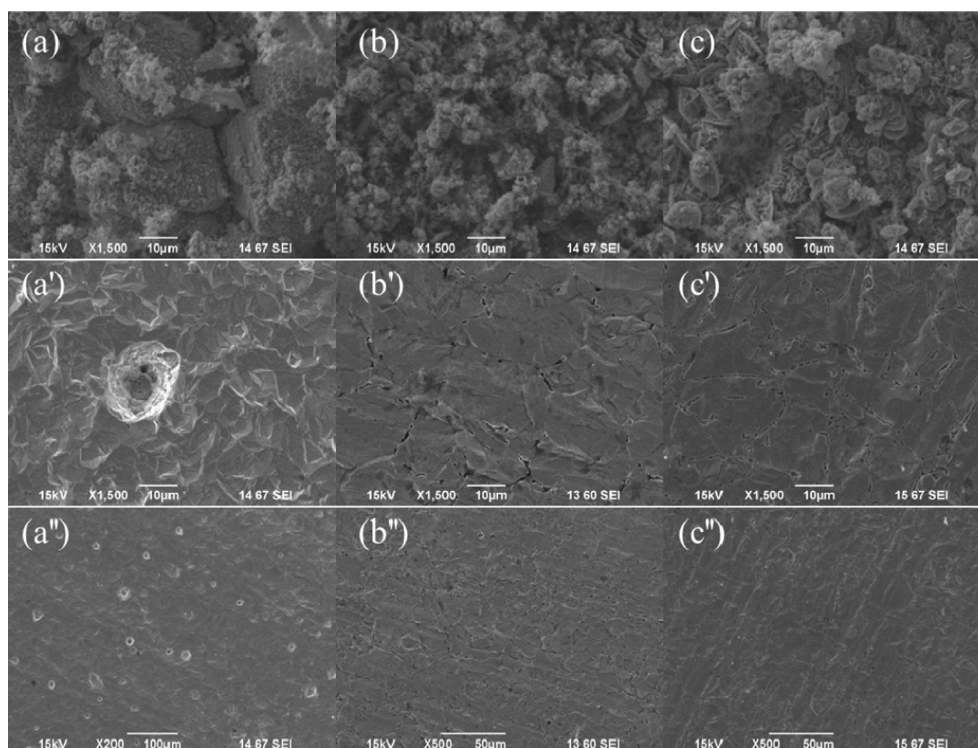


Fig. 4. SEM photos of Cu coupon surface morphologies before (a, b, c) and after removing corrosion products (a', b', c') at the end of 7th day incubation in anaerobic vials with different headspace volumes: (a, a') 10 mL, (b, b') 85 mL, (c, c') 160 mL.

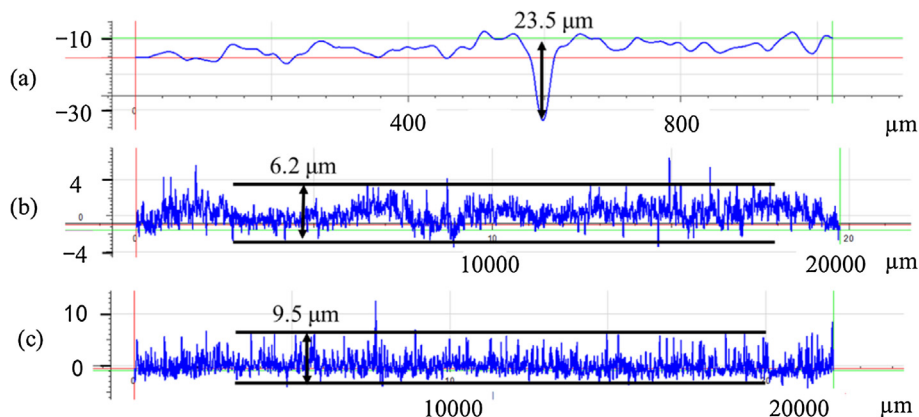


Fig. 5. Pit depth profiles of Cu coupons after removing biofilm and corrosion products at the end of 7th day incubation in anaerobic vial with 10 mL (a), 85 mL (b) and 160 mL (c) headspace volumes.

Fig. 6 shows the XRD patterns of the corrosion products on the surface of the Cu coupon from the vial with 85 mL headspace vs. the standard Cu_2S patterns. The XRD patterns of coupons in vials with headspace volumes of 10 mL and 160 mL were similar and thus omitted.

3.2. Dissolved H_2S concentration and weight loss

Fig. 7 shows that the H_2S concentrations in the headspace and pH in the broth after 7-day incubation of SRB with different headspace volumes. With the increase of the headspace volume, the broth pH increased from 6.96 to 7.34, while the concentration of H_2S in the headspace decreased from 450 ppm (v/v) to 280 ppm.

The weight losses of the Cu coupons after the 7-day incubation with different headspace volumes are shown in Fig. 8. Fig. 8 suggests that the weight loss decreased gradually with the increase in the headspace volume. Corresponding to headspace volumes of 10 mL, 85 mL and 160 mL, the weight losses of the Cu coupons were 23.0 mg/cm^2 , 18.7 mg/cm^2 , and 6.2 mg/cm^2 , respectively. The abiotic weight loss in the deoxygenated ATCC 1249 medium without inoculation was found to be negligible in a previous study [61]. For 10 mL headspace, the 23.0 mg/cm^2 weight loss and 23.5 μm maximum pit depth yielded a relative pitting severity $RPS = 0.92$,

indicating that both pitting corrosion and uniform corrosion were almost equally important. For 85 mL headspace and 160 mL space, there was no significant pitting ($RPS \approx 0$). For SRB MIC of carbon steel, a much larger than unity RPS value of 6.8 was reported [61], indicating that pitting corrosion was far more important than uniform corrosion.

3.3. Electrochemical measurements

Fig. 9 shows the trend of OCP of Cu vs. time for the three different headspace volumes. The OCP curves for all the three headspace volumes show an increasing trend with time. More importantly, OCP curve for the 10 mL headspace was at the bottom while that for 160 mL on top. Fig. 10 shows the data of the linear polarization resistance (R_p) vs. time for the three different headspace volumes. In all cases, R_p increased and then decreased during the 7-day incubation period. With the increase of the headspace volume, R_p increased, indicating increased corrosion resistance (i.e., decreased corrosion rate) for a larger headspace volume. The lowest R_p (149 $\Omega \text{ cm}^2$) was found in the vial with 10 mL headspace on the 1st day while the highest R_p (328 $\Omega \text{ cm}^2$) in the vial with 160 mL headspace on the 5th day.

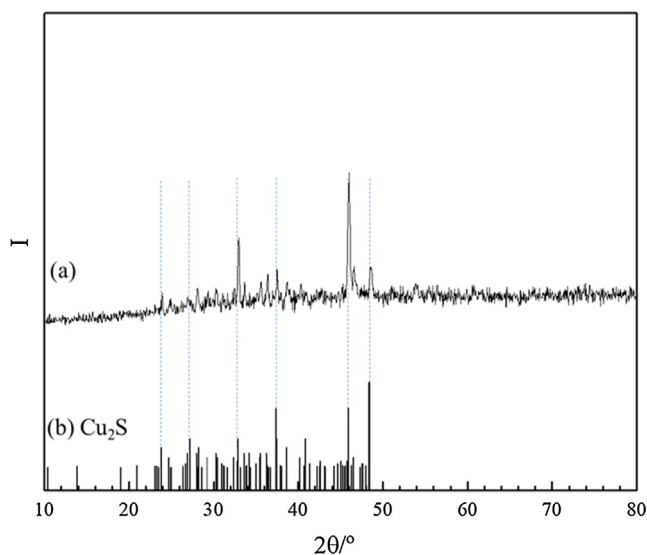


Fig. 6. XRD patterns of corrosion products after 7-day incubation in anaerobic vial with 85 mL headspace volume (a) vs. XRD standard patterns of Cu_2S (b).

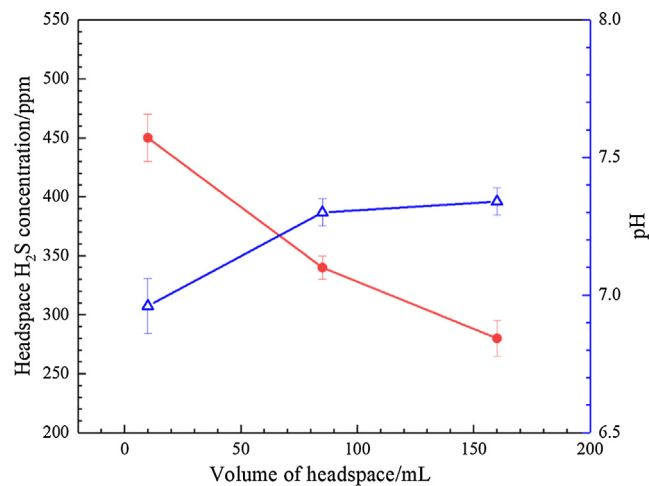


Fig. 7. H_2S concentration (circle) in headspace and pH (triangle) in 40 mL broth after 7-day incubation in anaerobic vials with different headspace volumes (10 mL, 85 mL, 160 mL).

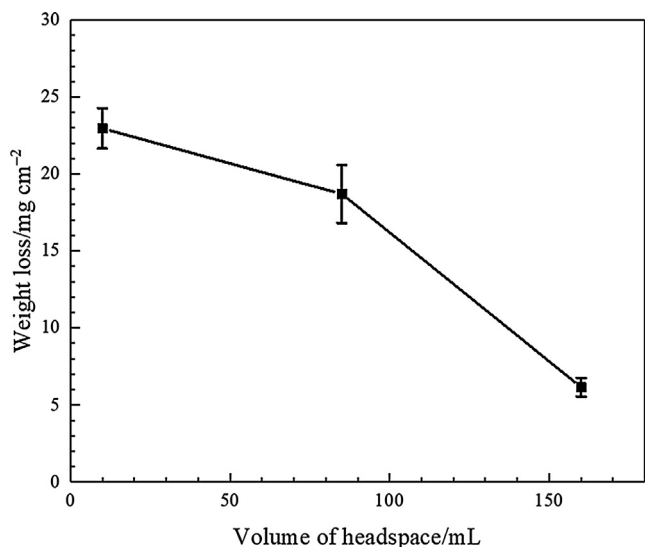


Fig. 8. Weight losses of the Cu coupons after 7-day incubation in anaerobic vials with different headspace volumes (10 mL, 85 mL, 160 mL).

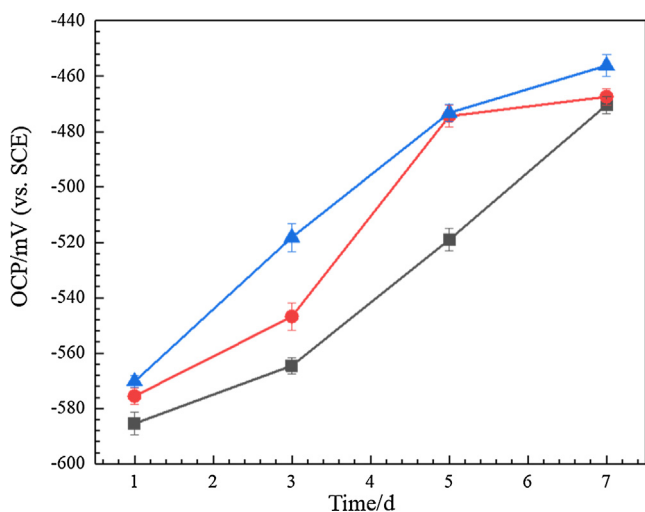


Fig. 9. OCP curves of Cu after 7-day incubation in electrochemical glass cells with headspace volumes of 10 mL (square), 85 mL (circle) and 160 mL (triangle).

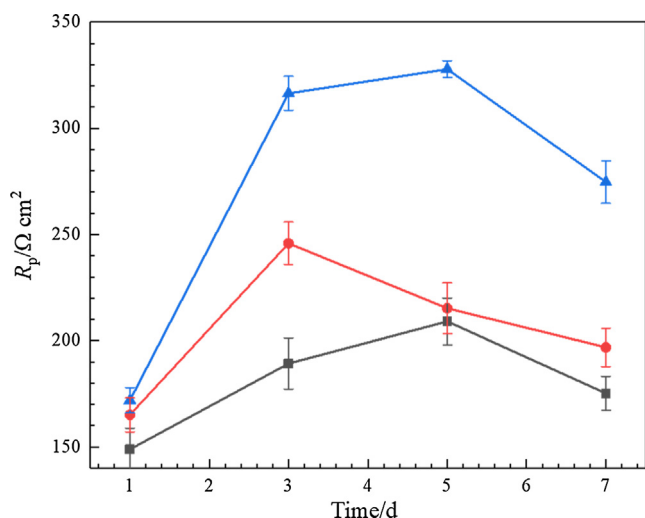


Fig. 10. Linear polarization resistance (R_p) curves of Cu coupons after 7-day incubation in electrochemical glass cells with headspace volumes of 10 mL (square), 85 mL (circle) and 160 mL (triangle).

Fig. 11 shows the Nyquist and Bode plots of Cu at the end of 7th day. The Nyquist plots include a capacitive loop at the high frequency range and a Warburg impedance line at the lower frequency range. In the Bode plots, the impedance for the headspace volume of 160 mL is higher than those for 85 mL and 10 mL. The impedance for 10 mL headspace was a little lower than that for 85 mL headspace. Equivalent electrical circuit fitting results of the EIS spectra are displayed in Scheme 1, in which R_s , R_b , R_f and R_{ct} stand for solution resistance, biofilm resistance, corrosion product film resistance and charge transfer resistance, respectively. Q_b and Q_f are constant phase elements (CPEs) of the biofilm and the corrosion product film, respectively, and Z_w Warburg impedance. C_{dl} represents capacitance of the electrical double layer.

Table 1 lists the parameters derived from EIS fitting using the electrical circuits. R_{ct} increased with the increase in headspace volume, indicating a lower corrosion rate for a larger headspace volume. The smallest R_{ct} occurred for 10 mL headspace. In EIS modeling, the impedance of a constant phase element (CPE) is derived from the following equation,

$$Z_Q = Y_0^{-1}(j\omega)^{-n} \quad (12)$$

where ω is angular frequency in rad/s and j unit imaginary number. Y_0 and n are CPE parameters [47].

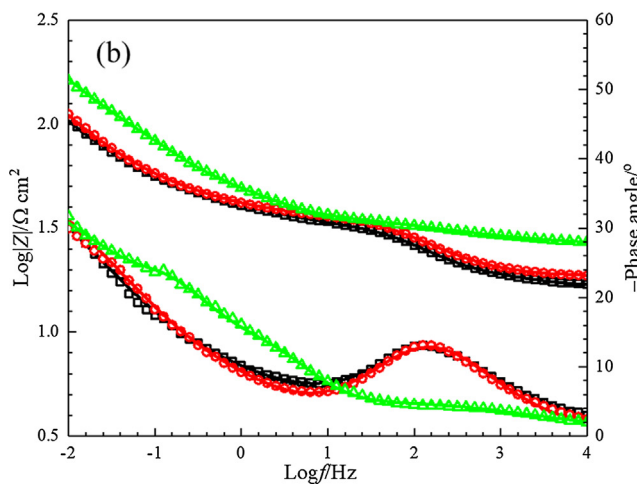
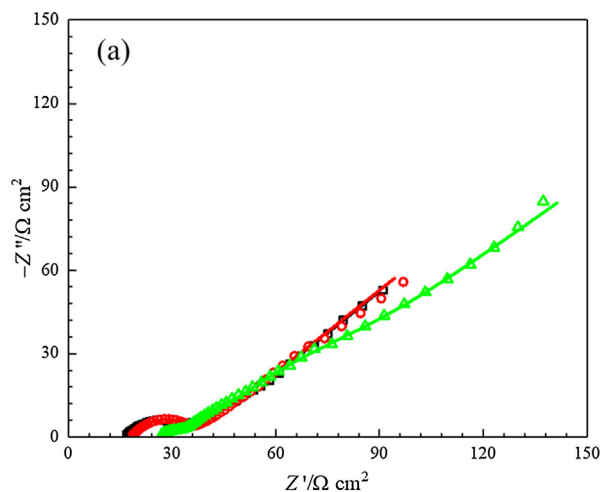
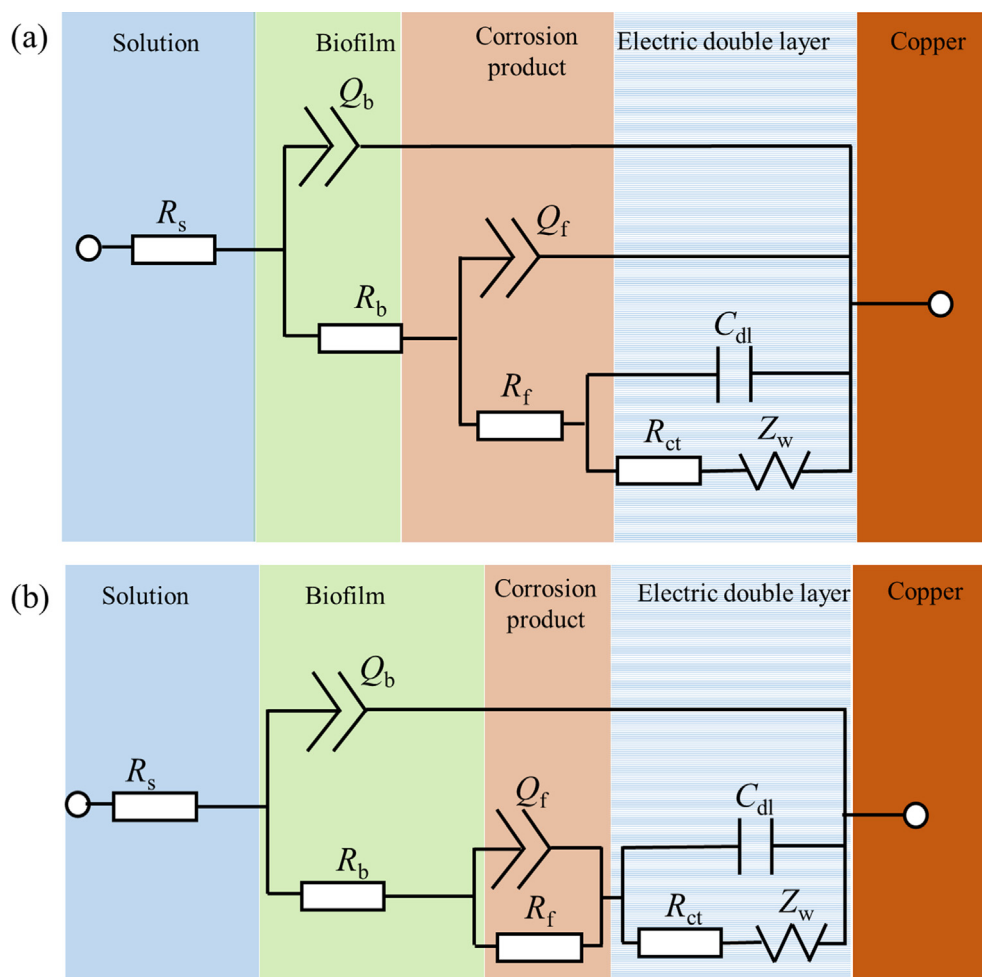


Fig. 11. Nyquist (a) and Bode (b) plots of Cu after 7-day incubation in electrochemical glass cells with headspace volumes of 10 mL (square), 85 mL (circle) and 160 mL (triangle).

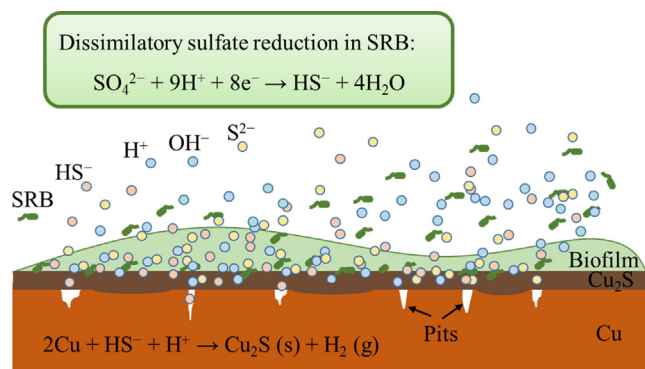


Scheme 1. Equivalent circuit for fitting EIS spectra after 7-day incubation in electrochemical glass cells with different headspace volumes: (a) 10 mL and 85 mL, (b) 160 mL.

Table 1

Parameters derived from fitting EIS spectra using equivalent electrical circuits after 7-day incubation with different headspace volumes.

Headspace (mL)	R_s ($\Omega \text{ cm}^2$)	Y_b ($\Omega^{-1} \text{ cm}^{-2} \text{ s}^n$)	n_b	R_b ($\Omega \text{ cm}^2$)	Y_f ($\Omega^{-1} \text{ cm}^{-2} \text{ s}^n$)	n_f	R_f ($\Omega \text{ cm}^2$)	C_{dl} (F)	R_{ct} ($\Omega \text{ cm}^2$)	Z_w ($\Omega^{-1} \text{ cm}^{-2} \text{ s}^{0.5}$)
10	16.4	1.2×10^{-5}	0.95	1.55	7.8×10^{-4}	0.68	18.2	8.6×10^{-3}	4.0	0.054
85	18.3	1.7×10^{-5}	0.99	1.96	5.2×10^{-4}	0.73	17.4	9.3×10^{-3}	5.6	0.049
160	25.5	6.2×10^{-3}	0.40	16.2	6.8×10^{-2}	0.99	19.2	2.5×10^{-3}	16.1	0.024



Scheme 2. The mechanism of SRB MIC on Cu corrosion.

4. Discussion

The mechanism of Cu corrosion by SRB is illustrated in Scheme 2. The metabolite HS^- was from H_2S secreted by SRB. It

can be decomposed to H^+ and S^{2-} or combine with H^+ to form H_2S [61]. The HS^- diffused to Cu surface and reacted with Cu to produce Cu_2S . The biofilm complicated the interface between Cu and the electrolyte and thus promoted heterogeneity of the Cu surface.

With a fixed broth volume of 40 mL in all vials, a larger headspace means that more H_2S in the broth escaped to the headspace, which made the broth less toxic to SRB [45]. Thus, both planktonic and sessile SRB cells grew better as evidenced by the increased planktonic and sessile cell counts (Fig. 2) and the denser biofilms in the CLSM images (Fig. 3). Because the escaped H_2S took away more H^+ from the broth as shown in Reaction (4), Fig. 7 shows that the broth pH increased with the increase in the headspace volume.

Fig. 7 shows that with a decrease in the headspace volume, H_2S in the headspace became more concentrated due to the smaller headspace volume with less dilution of H_2S . Vapor-liquid equilibrium for H_2S dictates that the corresponding dissolved H_2S concentration in the broth should increase with the smallest 10 mL headspace having the highest dissolved $[\text{H}_2\text{S}]$ and 160 mL headspace having the lowest. Because Cu corrosion by SRB belongs to

M-MIC, the increased dissolved $[H_2S]$ directly resulted in more weight loss (Fig. 7). The trend of decreasing weight loss following the increase in headspace volume for Cu MIC by SRB is completely the opposite to that in carbon steel MIC by SRB reported by Jia et al. [45]. Carbon steel MIC by SRB is due to EET-MIC with SRB cells harvesting extracellular electrons from the iron matrix for energy. The increased headspace volume led to less H_2S toxicity in the broth and thus a higher sessile cell count [45].

Because Cu is much more noble than carbon steel [61], it cannot serve as an electron donor for sulfate reduction. In this work, Cu was corroded by the main metabolite of SRB, i.e. H_2S [57,65]. The XRD analysis of the corrosion product in Fig. 6 confirmed the corrosion product (Cu_2S) in the Cu corrosion Reaction (7). OCP shows the thermodynamic tendency of the working electrode to be corroded. Fig. 9 shows that the OCP for 10 mL headspace was the most negative, indicating a higher thermodynamic tendency for corrosion for a smaller headspace volume. R_p provides kinetic corrosion trend. Fig. 10 shows that 10 mL headspace had the lowest R_p , corresponding to the highest corrosion rate. This corrosion trend is consistent with the weight loss trend (Fig. 8). In Fig. 10, the R_p curves for all the three headspace volumes increased first and then decreased after 3 days of incubation. It indicates that corrosion rate decreased first and then increased afterwards. The build-up of a corrosion product film hindered Cu dissolution. However, when the biofilm became more mature with more extracellular polymeric substances (EPS) in the biofilm matrix, the local concentrations of HS^- and H^+ started to increase under the biofilm enclosure, leading to an increase of the corrosion rate.

The EIS results in Table 1 also show that 10 mL headspace had the lowest corrosion resistance. The Warburg impedance (Z_w) indicated that Cu^+ ion diffusion from Cu to the bulk solution hindered corrosion. Thus, the Z_w values for headspace volumes of 10 mL and 85 mL were significantly higher than that of 160 mL. It is worth noting that R_{ct} in this work was much lower than that in carbon steel MIC by *D. vulgaris* reported by Jia et al. [45]. This explains why the Cu weight loss (mg/cm^2) in this work is an order of magnitude higher than that for carbon steel [45].

Chen et al. investigated abiotic Cu corrosion by sulfide. They found that the Cu corrosion rate was controlled by diffusion of HS^- [66–68]. The corrosion mode was mainly uniform corrosion. No obvious corrosion pits were found. Interestingly, in this work, pits as deep as 23.5 μm were found on the Cu surface for 10 mL headspace, which had the highest concentration of dissolved $[H_2S]$. Underneath the biofilm, the sulfide concentration could be much higher than in the broth, because the sessile cells' volumetric density was typically 10^2 to 10^3 times higher than that of the planktonic cells in the broth.

No well-defined large pits were found on Cu with headspace volumes of 85 mL and 160 mL, but distinct intergranular corrosion patterns are seen in SEM images (Fig. 4). The grain size “carved” out by the intergranular corrosion shown in Fig. 4(b’,c”) is roughly 40 μm , which matches that reported for 110 Cu [69]. The atoms on the crystal boundary have increased free energy and higher diffusion rate than the atoms in the center of the crystal [70,71]. Thus, the crystal boundary was easier to be corroded than the center of crystal. This work for the first time reports this very interesting phenomenon in Cu MIC, suggesting that the pattern of Cu corrosion by biogenic sulfide depends on sulfide concentration.

5. Conclusion

This study investigated corrosion of Cu by *D. vulgaris* in anaerobic vials with different headspace volumes and a fixed broth volume of 40 mL that resulted in different dissolved $[H_2S]$ and cell counts after 7 days of incubation. A larger headspace led to more H_2S escaped to the headspace and thus less sulfide toxicity in the

broth. This allowed better planktonic and sessile cell growth. However, Cu corrosion severity decreased, opposite to the increase trend in carbon steel corrosion by the same SRB, because Cu MIC by SRB belongs to M-MIC by secreted sulfide and the smallest headspace volume (10 mL) had the most concentrated sulfide, while for carbon steel, EET-MIC is the main mechanism. In this work, uniform corrosion was accompanied by severe pitting when the dissolved $[H_2S]$ was high in the vial with a 10 mL headspace. In the vials with 85 mL and 160 mL headspace volumes, the dissolved H_2S concentrations were lower, leading to uniform corrosion accompanied by intergranular corrosion. LPR, potentiodynamic polarization resistance and EIS data corroborated the weight loss corrosion data trend.

Declaration of Competing Interest

The authors declare that they have no known competing financial interests or personal relationships that could have appeared to influence the work reported in this paper.

Acknowledgements

WD acknowledges China Postdoctoral Science Foundation (Grant No. 2018M640655 and 2019T120610), Open Fund of Shandong Key Laboratory of Corrosion Science (Grant No. KLCS201903) and the China Scholarship Council for financial supports to do research at Ohio University. WD and SC acknowledge the financial support by the National Natural Science Foundation of China (Grant Nos. 51572249 and U1806223).

References

- [1] B. Hou, X. Li, X. Ma, C. Du, D. Zhang, M. Zheng, W. Xu, D. Lu, F. Ma, The cost of corrosion in China, *npj Mater. Degrad.* 1 (2017) 1–9.
- [2] X. Li, D. Zhang, Z. Liu, Z. Li, C. Du, C. Dong, Share corrosion data, *Nature* 527 (2015) 441.
- [3] R.H. Gaines, Bacterial activity as a corrosive influence in the soil, *Ind. Eng. Chem.* 2 (1910) 128–130.
- [4] R. Javaherdashti, A review of some characteristics of MIC caused by sulfate-reducing bacteria: past, present and future, *Anti-Corros. Methods Mater.* 46 (1999) 173–180.
- [5] H. Liu, T. Gu, G. Zhang, Y. Cheng, H. Wang, H. Liu, The effect of magnetic field on biomineralization and corrosion behavior of carbon steel induced by iron-oxidizing bacteria, *Corros. Sci.* 102 (2016) 93–102.
- [6] H. Wang, L.-K. Ju, H. Castaneda, G. Cheng, B.-M. Zhang Newby, Corrosion of carbon steel C1010 in the presence of iron oxidizing bacteria *Acidithiobacillus ferrooxidans*, *Corros. Sci.* 89 (2014) 250–257.
- [7] Z. Guo, T. Liu, Y.F. Cheng, N. Guo, Y. Yin, Adhesion of *Bacillus subtilis* and *Pseudoalteromonas lipolytica* to steel in a seawater environment and their effects on corrosion, *Colloids Surf., B* 157 (2017) 157–165.
- [8] S. Li, L. Li, Q. Qu, Y. Kang, B. Zhu, D. Yu, R. Huang, Extracellular electron transfer of *Bacillus cereus* biofilm and its effect on the corrosion behaviour of 316L stainless steel, *Colloids Surf., B* 173 (2019) 139–147.
- [9] Y. Leckbach, Z. Li, D. Xu, S. El Abed, Y. Dong, D. Liu, T. Gu, S.I. Koraichi, K. Yang, F. Wang, *Salvia officinalis* extract mitigates the microbiologically influenced corrosion of 304L stainless steel by *Pseudomonas aeruginosa* biofilm, *Bioelectrochemistry* 128 (2019) 193–203.
- [10] T. Gu, K. Zhao, S. Nestic, A Practical Mechanistic Model for MIC Based on a Biocatalytic Cathodic Sulfate Reduction Theory, Corrosion 2009, Paper No. 09390, March 2009, Atlanta, GA.
- [11] R. Jia, Y. Li, H.H. Al-Mahamedh, T. Gu, Enhanced biocide treatments with D-amino acid mixtures against a biofilm consortium from a water cooling tower, *Front. Microbiol.* 8 (2017) 1538.
- [12] J.I. Brauer, S. Celikkol-Aydin, J.A. Sunner, C.C. Gaylarde, I.B. Beech, Metabolomic imaging of a quaternary ammonium salt within a marine bacterial biofilm on carbon steel, *Int. Biodeterior. Biodegrad.* 125 (2017) 33–36.
- [13] M. Talha, Y. Ma, P. Kumar, Y. Lin, A. Singh, Role of protein adsorption in the bio corrosion of metallic implants – A review, *Colloids Surf., B* 176 (2019) 494–506.
- [14] J. Wang, F. Xiong, H. Liu, T. Zhang, Y. Li, C. Li, W. Xia, H. Wang, H. Liu, Study of the corrosion behavior of *Aspergillus niger* on 7075-T6 aluminum alloy in a high salinity environment, *Bioelectrochemistry* 129 (2019) 10–17.
- [15] H. Qian, D. Zhang, Y. Lou, Z. Li, D. Xu, C. Du, X. Li, Laboratory investigation of microbiologically influenced corrosion of Q235 carbon steel by halophilic archaea *Natronorubrum tibetense*, *Corros. Sci.* 145 (2018) 151–161.

- [16] T. Liu, Z. Guo, Z. Zeng, N. Guo, Y. Lei, T. Liu, S. Sun, X. Chang, Y. Yin, X. Wang, Marine bacteria provide lasting anti-corrosion activity for steel via biofilm-induced mineralization, *ACS Appl. Mater. Interfaces* 10 (2018) 40317–40327.
- [17] H. Liu, T. Gu, G. Zhang, H. Liu, Y.F. Cheng, Corrosion of X80 pipeline steel under sulfate-reducing bacterium biofilms in simulated CO₂-saturated oilfield produced water with carbon source starvation, *Corros. Sci.* 136 (2018) 47–59.
- [18] S. Sun, S. Tang, X. Chang, N. Wang, D. Wang, T. Liu, Y. Lei, Y. Zhu, A bifunctional melamine sponge decorated with silver-reduced graphene oxide nanocomposite for oil-water separation and antibacterial applications, *Appl. Surf. Sci.* 473 (2019) 1049–1061.
- [19] A.N. Ilyaletdinov, P.B. Enker, L.V. Loginova, Role of sulfate-reducing bacteria in precipitation of copper, *Mikrobiologiya* 46 (1977) 92–95.
- [20] S.W. Borenstein, P.B. Lindsay, Microbiologically influenced corrosion failure analyses, *Mater. Perform.* 27 (1988) 51–54.
- [21] J. Xu, R. Jia, D. Yang, C. Sun, T. Gu, Effects of d-Phenylalanine as a biocide enhancer of THPS against the microbiologically influenced corrosion of C1018 carbon steel, *J. Mater. Sci. Technol.* 35 (2019) 109–117.
- [22] T. Wu, C. Sun, J. Xu, M. Yan, F. Yin, W. Ke, A study on bacteria-assisted cracking of X80 pipeline steel in soil environment, *Corros. Eng., Sci. Technol.* 53 (2018) 265–275.
- [23] H. Liu, C. Fu, T. Gu, G. Zhang, Y. Lv, H. Wang, H. Liu, Corrosion behavior of carbon steel in the presence of sulfate reducing bacteria and iron oxidizing bacteria cultured in oilfield produced water, *Corros. Sci.* 100 (2015) 484–495.
- [24] D. Xu, Y. Li, F. Song, T. Gu, Laboratory investigation of microbiologically influenced corrosion of C1018 carbon steel by nitrate reducing bacterium *Bacillus licheniformis*, *Corros. Sci.* 77 (2013) 385–390.
- [25] E. Zhou, H. Li, C. Yang, J. Wang, D. Xu, D. Zhang, T. Gu, Accelerated corrosion of 2304 duplex stainless steel by marine *Pseudomonas aeruginosa* biofilm, *Int. Biodeterior. Biodegrad.* 127 (2018) 1–9.
- [26] H. Liu, Y.F. Cheng, Microbial corrosion of X52 pipeline steel under soil with varied thicknesses soaked with a simulated soil solution containing sulfate-reducing bacteria and the associated galvanic coupling effect, *Electrochim. Acta* 266 (2018) 312–325.
- [27] I.B. Beech, J. Sunner, Biocorrosion: towards understanding interactions between biofilms and metals, *Curr. Opin. Biotechnol.* 15 (2004) 181–186.
- [28] W. Lee, Z. Lewandowski, P.H. Nielsen, W.A. Hamilton, Role of sulfate-reducing bacteria in corrosion of mild-steel - a review, *Biofouling* 8 (1995) 165–194.
- [29] C.A.H. Wolzogen Kühr, L.S.V.d. Vlugt, The graphitization of cast iron as an electrochemical process in anaerobic soil, *Water* 18 (1934) 147–165.
- [30] R. King, J. Miller, J. Smith, Corrosion of mild steel by iron sulphides, *Br. Corros. J.* 8 (1973) 137–141.
- [31] W. Iverson, G. Olson, Anaerobic corrosion by sulfate-reducing bacteria due to a highly-reactive volatile phosphorus compound, Final report (1983).
- [32] H.T. Dinh, J. Kuever, M. Mußmann, A.W. Hassel, M. Stratmann, F. Widdel, Iron corrosion by novel anaerobic microorganisms, *Nature* 427 (2004) 829–832.
- [33] Y. Li, D. Xu, C. Chen, X. Li, R. Jia, D. Zhang, W. Sand, F. Wang, T. Gu, Anaerobic microbiologically influenced corrosion mechanisms interpreted using bioenergetics and bioelectrochemistry: A review, *J. Mater. Sci. Technol.* 34 (2018) 1713–1718.
- [34] D. Xu, Y. Li, T. Gu, Mechanistic modeling of biocorrosion caused by biofilms of sulfate reducing bacteria and acid producing bacteria, *Bioelectrochemistry* 110 (2016) 52–58.
- [35] T. Gu, New understandings of biocorrosion mechanisms and their classifications, *J. Microbiol. Biochem. Technol.* 4 (2012) iii–vi.
- [36] T. Gu, R. Jia, T. Unsal, D. Xu, Toward a better understanding of microbiologically influenced corrosion cause by sulfate reducing bacteria, *J. Mater. Sci. Technol.* 35 (2018) 631–636.
- [37] G. Reguera, K.D. McCarthy, T. Mehta, J.S. Nicoll, M.T. Tuominen, D.R. Lovley, Extracellular electron transfer via microbial nanowires, *Nature* 435 (2005) 1098.
- [38] S. Da Silva, R. Basséguy, A. Bergel, The role of hydrogenases in the anaerobic microbiologically influenced corrosion of steels, *Bioelectrochemistry* 56 (2002) 77–79.
- [39] M. Li, M. Zhou, X. Tian, C. Tan, C.T. McDaniel, D.J. Hassett, T. Gu, Microbial fuel cell (MFC) power performance improvement through enhanced microbial electrogenicity, *Biotechnol. Adv.* 36 (2018) 1316–1327.
- [40] P. Zhang, D. Xu, Y. Li, K. Yang, T. Gu, Electron mediators accelerate the microbiologically influenced corrosion of 304 stainless steel by the *Desulfovibrio vulgaris* biofilm, *Bioelectrochemistry* 101 (2015) 14–21.
- [41] R. Jia, D. Yang, D. Xu, T. Gu, Electron transfer mediators accelerated the microbiologically influence corrosion against carbon steel by nitrate reducing *Pseudomonas aeruginosa* biofilm, *Bioelectrochemistry* 118 (2017) 38–46.
- [42] Y. Huang, E. Zhou, C. Jiang, R. Jia, S. Liu, D. Xu, T. Gu, F. Wang, Endogenous phenazine-1-carboxamide encoding gene *PhzH* regulated the extracellular electron transfer in biocorrosion of stainless steel by marine *Pseudomonas aeruginosa*, *Electrochem. Commun.* 94 (2018) 9–13.
- [43] R.K. Thauer, E. Stackebrandt, W.A. Hamilton, Energy metabolism and phylogenetic diversity of sulphate-reducing bacteria, in: L.L. Barton, W.A. Hamilton (Eds.), *Sulphate-reducing bacteria: Environmental and engineered systems*, Cambridge University Press, Cambridge, UK, 2007, pp. 1–37.
- [44] D. Xu, T. Gu, Carbon source starvation triggered more aggressive corrosion against carbon steel by the *Desulfovibrio vulgaris* biofilm, *Int. Biodeterior. Biodegrad.* 91 (2014) 74–81.
- [45] R. Jia, J.L. Tan, P. Jin, D.J. Blackwood, D. Xu, T. Gu, Effects of biogenic H₂S on the microbiologically influenced corrosion of C1018 carbon steel by sulfate reducing *Desulfovibrio vulgaris* biofilm, *Corros. Sci.* 130 (2018) 1–11.
- [46] R. Jia, D. Wang, P. Jin, T. Unsal, D. Yang, J. Yang, D. Xu, T. Gu, Effects of ferrous ion concentration on microbiologically influenced corrosion of carbon steel by sulfate reducing bacterium *Desulfovibrio vulgaris*, *Corros. Sci.* (2019), <https://doi.org/10.1016/j.corsci.2019.03.038>.
- [47] W. Dou, J. Liu, W. Cai, D. Wang, R. Jia, S. Chen, T. Gu, Electrochemical investigation of increased carbon steel corrosion via extracellular electron transfer by a sulfate reducing bacterium under carbon source starvation, *Corros. Sci.* 150 (2019) 258–267.
- [48] M.B. Kleiner, S. Kuhn, K. Habeger, High performance forced air cooling scheme employing microchannel heat exchangers, *IEEE Trans. Compon. Packag. Manuf. Technol. Part A*: 18 (1995) 795–804.
- [49] J. Tian, T. Kim, T. Lu, H. Hodson, D. Queheillat, D. Sypeck, H. Wadley, The effects of topology upon fluid-flow and heat-transfer within cellular copper structures, *Int. J. Heat Mass Transf.* 47 (2004) 3171–3186.
- [50] J. Chen, Z. Qin, D. Shoesmith, Long-term corrosion of copper in a dilute anaerobic sulfide solution, *Electrochim. Acta* 56 (2011) 7854–7861.
- [51] J. Smith, Z. Qin, F. King, L. Werme, D. Shoesmith, Sulfide film formation on copper under electrochemical and natural corrosion conditions, *CORROSION* 63 (2007) 135–144.
- [52] E. Huttunen-Saarivirta, P. Rajala, M. Bomberg, L. Carpén, EIS study on aerobic corrosion of copper in ground water: influence of micro-organisms, *Electrochim. Acta* 240 (2017) 163–174.
- [53] G.T. Burstein, H. Bi, G. Kawaley, The persistence of inhibition of copper corrosion in tap water, *Electrochim. Acta* 191 (2016) 247–255.
- [54] S. Chen, D. Zhang, Study of corrosion behavior of copper in 3.5 wt.% NaCl solution containing extracellular polymeric substances of an aerotolerant sulphate-reducing bacteria, *Corros. Sci.* 136 (2018) 275–284.
- [55] A. Jayaraman, D. Ornek, D. Duarte, C.-C. Lee, F. Mansfeld, T. Wood, Axenic aerobic biofilms inhibit corrosion of copper and aluminum, *Appl. Microbiol. Biotechnol.* 52 (1999) 787–790.
- [56] F. Mansfeld, B. Little, Microbiologically influenced corrosion of copper-based materials exposed to natural seawater, *Electrochim. Acta* 37 (1992) 2291–2297.
- [57] E. Huttunen-Saarivirta, P. Rajala, L. Carpén, Corrosion behaviour of copper under biotic and abiotic conditions in anoxic ground water: electrochemical study, *Electrochim. Acta* 203 (2016) 350–365.
- [58] I.G. Petrisor, A. Kanner, Chinese Drywall—Environmental Forensic Opportunities, *Environ. Forensics* 11 (2010) 6–16.
- [59] S. Chen, P. Wang, D. Zhang, Corrosion behavior of copper under biofilm of sulfate-reducing bacteria, *Corros. Sci.* 87 (2014) 407–415.
- [60] G. Huang, K.Y. Chan, H.H.P. Fang, Microbiologically induced corrosion of 70Cu30Ni alloy in anaerobic seawater, *J. Electrochem. Soc.* 151 (2004) B434–B439.
- [61] W. Dou, R. Jia, P. Jin, J. Liu, S. Chen, T. Gu, Investigation of the mechanism and characteristics of copper corrosion by sulfate reducing bacteria, *Corros. Sci.* 144 (2018) 237–248.
- [62] J. Chen, Z. Qin, D.W. Shoesmith, Kinetics of corrosion film growth on copper in neutral chloride solutions containing small concentrations of sulfide, *J. Electrochem. Soc.* 157 (2010) C338.
- [63] R. Jia, D. Yang, Y. Li, D. Xu, T. Gu, Mitigation of the *Desulfovibrio vulgaris* biofilm using alkyltrimethylbenzylammonium chloride enhanced by d-amino acids, *Int. Biodeterior. Biodegrad.* 117 (2017) 97–104.
- [64] A.C.G.-o.C.o. Metals, Standard practice for preparing, cleaning, and evaluating corrosion test specimens, *ASTM International*, 2011.
- [65] I. Puigdomenech, C. Taxén, Thermodynamic data for copper. Implications for the corrosion of copper under repository conditions, *Swedish Nuclear Fuel and Waste Management Co*, 2000.
- [66] J. Chen, Z. Qin, T. Martino, M. Guo, D.W. Shoesmith, Copper transport and sulphide sequestration during copper corrosion in anaerobic aqueous sulphide solutions, *Corros. Sci.* 131 (2018) 245–251.
- [67] J. Chen, Z. Qin, T. Martino, D.W. Shoesmith, Non-uniform film growth and micro/macro-galvanic corrosion of copper in aqueous sulphide solutions containing chloride, *Corros. Sci.* 114 (2016).
- [68] J. Chen, Z. Qin, L. Wu, J.J. Noël, D.W. Shoesmith, The influence of sulphide transport on the growth and properties of copper sulphide films on copper, *Corros. Sci.* 87 (2014) 233–238.
- [69] W. Chan, M. Fu, J. Lu, J. Liu, Modeling of grain size effect on micro deformation behavior in micro-forming of pure copper, *Mater. Sci. Eng., A* 527 (2010) 6638–6648.
- [70] H. Miyamoto, K. Ikeuchi, T. Mimaki, The role of grain boundary plane orientation on intergranular corrosion of symmetric and asymmetric [110] tilt grain boundaries in directionally solidified pure copper, *Scr. Mater.* 50 (2004) 1417–1421.
- [71] M. Yamashita, T. Mimaki, S. Hashimoto, S. Miura, Intergranular corrosion of copper and α -Cu-Al alloy bicrystals, *Philos. Mag. A* 63 (1991) 695–705.